Design and optimization of a blue fluorescent microcavity-organic light-emitting diode (MOLED) on AZO anode for an algae excitation light source application

L.A. Lozano-Hernández, Benjamin Reig, Jean Baptiste Doucet, Ludovic Salvagnac, Stéphane Calvez, H.Y. Lee, C.T. Lee, Isabelle Séguy, Véronique Bardinal

Design and optimization of a blue fluorescent microcavity-organic light-emitting diode (MOLED) on AZO anode for an algae excitation light source application

L.A. Lozano-Hernández[a], J.B. Doucet[a], B. Reig[a], L. Salvagnac[a], H.Y. Lee[b], C.T. Lee[b,c,d], S. Calvez[a], I. Séguy[a]1, V. Bardinal[a]

[a]*LAAS-CNRS, 7 avenue du colonel Roche, 31400 Toulouse, France*
[b]*Department of Photonics, National Cheng Kung University, Tainan 701, Taiwan, Republic of China*
[c]*Institute of Microelectronics, Department of Electrical Engineering, National Cheng Kung University, Taiwan 701, Taiwan, Republic of China*
[d]*Department of Electrical Engineering, Yuan Ze University, Taoyuan 320, Taiwan, Republic of China*

Abstract

In this work, we present simultaneous organic light-emitting diode (OLED) stack optimization and optical modelling for a blue microcavity-OLED (MOLED) based on AZO anode to be used as algae excitation light in optical biosensor. Fluorescent materials (MADN and DPAVBi) were chosen as host:guest for the doped emissive layer due their known stability compared to phosphorescent and thermally activated delayed fluorescence (TADF) materials. The MOLED modelling was performed by targeting 470 nm as the maximal excitation wavelength and suppressing the emission in the algae fluorescence bandwidth (600-800 nm) in order to fulfil the sensor requirements. By using a bilayer hole transport layer/electron blocking layer (HTL/EBL) instead of a single HTL, the total thickness was adjusted to meet the resonance wavelength condition without loss of efficiency, while at the same time preserving a maximum electric field intensity in the emissive layer (antinode position). MOLED devices were fabricated by organic semiconductor evaporation on three dielectric distributed Bragg reflectors (DBRs) with 3 different numbers of TiO_2/SiO_2 (high-index/low-index) pairs and aluminum-doped zinc oxide (AZO) transparent electrode . Devices with 1.5 pairs as DBR showed not only an improved external quantum efficiency (+33%) compared to a standard OLED but also an increase of about 3 times the intensity of the peak at 470 nm combined to a lower emission in the 600-800 nm bandwidth, as aimed. This increase in the peak intensity should lead to a longer device lifetime, as the current density necessary to excite algae at 470 nm is significantly lower owing to the microcavity effect.

Keywords: Blue OLED; MOLED; DBR; AZO; biosensor; microcavity OLED

1. Introduction

Since C.W. Tang and S. A. VanSlyke publication in 1987[1], organic light emitting diodes (OLEDs) have been attracted scientific and commercial attention because of the versatility of their optical and mechanical properties such as color intensity, high contrast, wide viewing angles, flexibility, lightness…[2,3]. Nowadays, OLED are already widely commercialized in devices such as smartphones, TVs, smartwatches, etc. In addition, the advantages of OLED technology, allowing light source integration on many types of substrates, open up new and promising applications such as chemical and biological sensors [4]. However, even if organic LEDs are already commercialized, their stability and lifetimes are not yet comparable to their inorganic counterparts, preventing their use in sensors where device stability is mandatory [5]. This lack of stability is partly due to Indium diffusion in organic layers. In this context, aluminum zinc oxide electrode (AZO) constitutes a low-cost, nontoxic and relative abundant alternative anode to ITO (indium tin oxide) since Zn diffusion is much lower[6]. There was also increased research efforts on this issue, focusing on the synthesis of new molecules and on optimizing the extraction of emitted light [2]. With the development of different generation of emitting materials (such as fluorescent, phosphorescent, thermally activated delayed fluorescent – TADF and hyperfluorescent) OLEDs have now reached a higher efficiency, but the stability problem remains [7]. Indeed, while fluorescent OLEDs can achieve lifetimes of the order of tens of thousands of hours, newest and more efficient systems as the hyperfluorescent are limited, in general, to just a few hours[8]. Blue fluorescent OLEDs (first

* Corresponding author.
E-mail address: lalozanohe@laas.fr

generation of emitting materials) are still used in industry although they exhibit lower efficiency compared to the last materials generation [9].
As an additional improvement, several options to increase the outcoupling of light, the overall OLED efficiency and even tune the electroluminescence (EL) spectra of the device have been reported[10]. One of the most promising option is the microcavity-OLED (MOLED) based on the integration in the OLED stack of a distributed Bragg reflector (DBR) made of alternate layers of high and low refractive index[11]. In a classic OLED, with organic semiconductors (OSCs) sandwiched between a transparent anode and a metallic cathode, only about 20% of the emitted light (internal quantum efficiency, IQE) is extracted. Around 50 % of this light is lost through the anode and the organic layers while another 30 % is lost in the substrate (wave guided mode)[12]. So, it is possible to infer that theoretically, only around 5 % of the injected electrons will be extracted as photons (external quantum efficiency, EQE) for a fluorescent OLED (IQE_{max} ~ 25 %)[13]. Due to microcavity effect, the EL emission of MOLEDs can be easily filtered at a design wavelength and light intensity can be significantly improved for this wavelength [14].

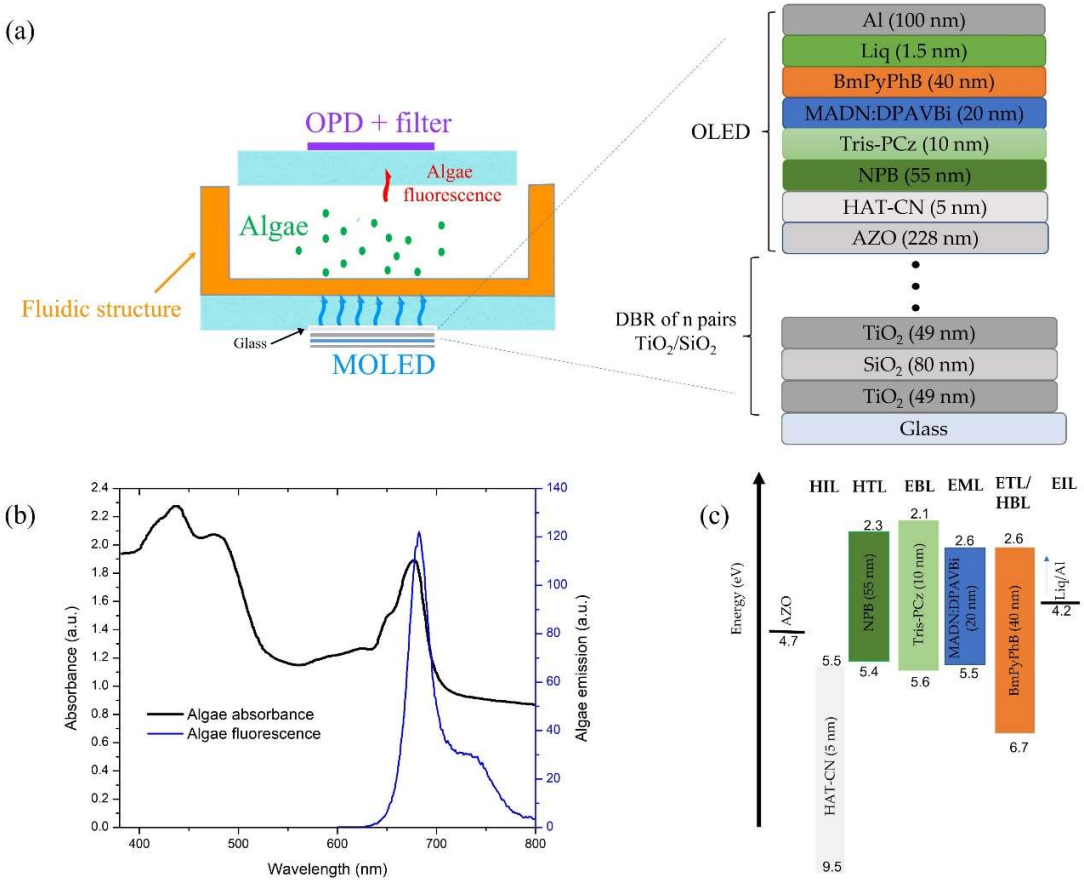

Fig. 1. (a) Schematic representation of the optical bio-sensor with MOLED structure, (b) algae absorbance and fluorescence spectra and (c) energy diagram for the OLED stack.

In this work we report on the design of a blue light source to be integrated in an optical biosensor dedicated to *in situ* monitoring of surface water quality. The system architecture consists of a fluidic structure with tanks and optical sensor (OLED and organic photodiode) located on its periphery (Fig. 1 (a)). The optical transducer will allow the detection of direct fluorescence emitted by green micro-algae at a wavelength of 680 nm (Fig. 1 (b)). The emission spectrum of classic OLEDs being wide, there could be significant spectral overlap between the signal to be detected and the emission tail of the OLED since the latter signal is of comparable intensity to that of algae fluorescence. So, the constraints related to algae fluorescence detection require the development of new device architecture for high efficiency (with a maximum emission matching algae absorption at 470 nm), reduced spectral width, and stable integrated deep blue OLED [15].

To that extent, a MOLED based on MADN:DPAVBi emitting layer (EML) and (TiO_2/SiO_2)-based DBR was designed. Here, the microcavity effect was exploited as a tool to fit the FWHM (full width at half maximum) of the OLED emission peak to the absorbance bandwidth of the algae (30nm). It was simultaneously used to reduce the OLED emission range in the algae fluorescence bandwidth (650-700 nm). Considering these specific spectral limits, we optimized both optically and electrically the spacers in the organic stack. Moreover, the MOLED was fabricated on an AZO anode deposited on the DBR to avoid the indium diffusion problem, which has not been done before. First, we investigated by modeling the variation of the two key parameters for the design of the MOLEDs: the optical cavity length (resonance condition) and the EML position relative to the electric field intensity (antinode position)[15]. A convergent solution for the optimal OLED and MOLED stacks, from the electronic and optical points of view, was found. Then, according to those results, OLED and MOLED devices were fabricated, characterized and compared.

2. Materials and methods

MOLEDs modelling was conducted by using a commercial software based on the matrix formalism[16]. Using this tool, it is possible to calculate the reflectivity and the transmission spectra of a multilayer stack if the refractive indices and thickness of each layer are known. To determine the real and imaginary refractive indices (n and k), ellipsometry measurements were conducted separately on each of the layers involved in the device and spectral models were derived from these data. To validate these models, full devices were then prepared on glass substrates coated with a 228 nm-thick AZO (Al-doped zinc oxide) or DBR/AZO anode on glass for OLED and MOLED respectively. The dielectric Bragg mirror was formed by a stack of 80 nm-thick low index (n~1.5) SiO_2 and 49 nm-thick high index (n~2.3) TiO_2 alternate layers. These thicknesses are chosen to be quarter-wave optical layers at the aimed resonance wavelength (470nm). Enclosing the organic region between this DBR/AZO part and a metallic electrode playing the role of the top mirror leads to the formation of a vertical micro-cavity. In such a device, the emitted light is confined and transmitted out of the cavity only for the resonance wavelengths (see modeling section). SiO_2 and TiO_2 materials were chosen for their high relative index contrast and their low absorption in the visible range and were deposited on the glass substrate by sputtering. AZO was deposited on the DBRs by atomic layer deposition technique (ALD). The deposition conditions were optimized to obtain a sheet resistance of 54 Ω/sq and a transmission of 79% [17] The reflectivity spectra of the DBR/AZO/glass stacks and their uniformity along the wafers were measured before MOLED fabrication and found in good agreement with modelling (not shown here).

AZO was patterned by chemical etching using standard photolithography. The substrates were cleaned with acetone and isopropanol 10 min each in an ultrasonic bath. Subsequently, UV-ozone treatment was performed for 10 min in order to remove any carbon contamination[18]. The OSC layers were sequentially evaporated at 5.10^{-7} torr with a rate of 0.03-0.05 nm/s in a Plassys MEB550B vacuum chamber installed in a glove box. The OLED/MOLED stack reported in Fig. 1 (a) is: 1,4,5,8,9,11-Hexaazatriphenylenehexacarbonitrile (HAT-CN) as hole injection layer (HIL), N,N'-Di(1-naphthyl)-N,N'-diphenyl-(1,1'-biphenyl)-4,4'-diamine (NPB) as hole transport layer (HTL), 9-Phenyl-3,6-bis(9-phenyl-9Hcarbazol-3-yl)-9H-carbazole (Tris-PCz) as electron blocking layer (EBL), 1,3-Bis(3,5-dipyrid-3-ylphenyl)benzene (BmPyPhB) as electron transport layer (ETL), 8-Hydroxyquinolinolato-lithium (Liq) as electron injection layer (EIL). For the EML 2-methyl-9,10-bis(naphthalen-2-yl)anthracene (MADN) was used as the host material doped with 4,4'-Bis[4-(di-*p*-tolylamino)styryl]biphenyl (DPAVBi). This layer was obtained by the co-evaporation of MADN and DPAVBi with a 4% doping level, controlled by the deposition rate of the two molecules (0.1 and 0.004 nm/s respectively). The 4% amount of DPAVBi has been set after a study of OLED efficiency vs doping ratio (not shown here). Aluminum was used as cathode and deposited at a rate of 1 nm/s. Finally, the devices were encapsulated with a cover glass sealed with epoxy adhesive inside the glove box.

After fabrication, J-L-V characterization and electroluminescence spectra were performed outside the glovebox by using a Keithley 2450 SourceMeter, an Irradian L203 photometer with a calibrated silicon photodetector and an Ocean Optics spectrometer respectively. External quantum efficiency calculations were made as reported by Shukla *et. Al*[19] by the J-L-V and EL spectra. The angular dependence of the EL intensity and corresponding spectra were also measured with a home-made set-up including a motorized goniometer.

3. Results and discussions

The Fig. 2 (a) displays the calculated reflectivity spectra of three different MOLEDs having 3 different numbers of pairs in the 470nm-centered DBR [17]. For each of them, the thickness of the organic stack was finely tuned to get an optical cavity length fully resonant at 470 nm. As a result, a sharp dip at 470 nm is obtained for each of them in the middle of the high reflectivity band comprised between 400 nm and 600 nm, which means light transmission will be

higher at 470 nm, as aimed. The FWHM (full width at half maximum) of the transmission peak will be also reduced compared to a standard OLED due to the microcavity effect. As seen, the FWHM is slightly varying with the number of pairs in the DBR and is equal to 26 nm for the 1.5 pairs-case. This spectral filtering is well suited to our pollution detection system application. One can also note that the reflectivity value at the resonance is not the same for the 3 cases, as it is mostly dependent of the balance between the bottom DBR reflectivity and the top aluminum electrode one. For the 1.5 pair case, this balance is almost perfect and the reflectivity at the resonance is close to zero. Consequently, light transmission through the transparent electrode will be optimal for this case and the MOLED efficiency is expected to be higher. A second reflectivity dip can be seen at 550nm~660nm, i.e. in a lower emission range of the OLED. It corresponds to the upper edge of the reflectivity stop band of the DBR and does not involve any amplification effect.The OLED stack was also optimized by carefully positioning the EML in such a way that it coincides to a maximum of the standing wave electric field in the multilayer stack (see Fig. 2 (b)) at an antinode position for which constructive interferences occur and light amplification is maximized. As observed, the magnitude and the distribution of the electrical field also depend on the number of pairs in the DBR. The most favorable case is again when a DBR with 1.5 pairs is used (MOLED 1.5: 44V/m) compared to the other cases (2.5 and 3.5, respectively 37V/m and 27V/m).

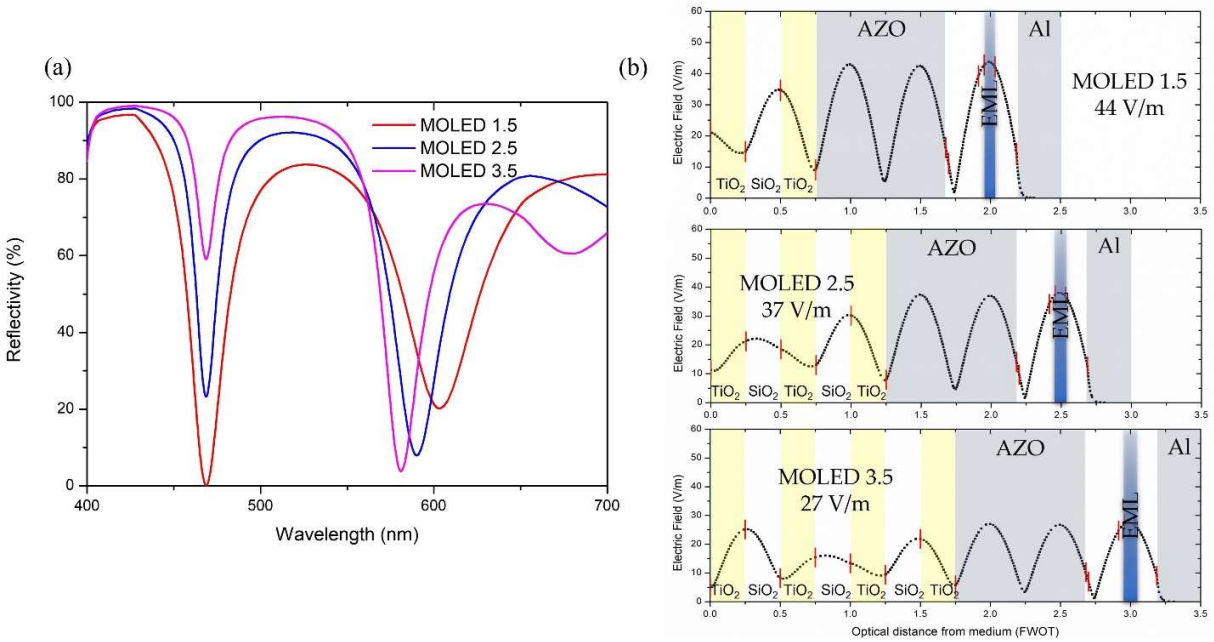

Fig. 2. (a) Reflectivity and (b) electric field obtained by model for the 3 types of MOLED by using a DBR with 1.5, 2.5 and 3.5 pairs.

The designed OLED stack, shown in Fig. 1 (a), was finely optimized to reach a solution meeting simultaneously the best OLED performances and MOLED optical design. In our case, according to the model results (Fig. 2 (b)), the latter condition is achieved for an EML layer located at 298 nm from the DBR mirror. In the literature, the most common selected method, was to adjust the cavity length by simply varying the thickness of the HTL, HIL or both. However, these devices architectures involve unusually thick layers of organic semiconductors that leads to a loss of performance and stability of the OLEDs[20]. Adachi et. Al[21] recently demonstrated that by modifying the HAT-CN layer from 10 nm to even 200 nm, it is possible to increase the overall OLED thickness while keeping the current density at the same value. Nevertheless, the EQE was significantly reduced from ~13 to ~9% corresponding to HAT-CN thicknesses of 10 and 200 nm respectively. Among these papers, one can note the use of a multi-layered HAT-CN(20 nm)/NPB(60 nm)/HAT-CN(15 nm)/NPB(60 nm) HTL[22] with a large thickness of 155 nm that fulfils the cavity length and at the same time enables an efficient hole transport by using two materials with excellent charge carrier mobility. In contrast, for a classic OLED the optimal thickness for HAT-CN and NPB is rather around 5-10 nm and 50 nm respectively[23,24]. In this work, Tris-PCz was introduced as EBL (Fig. 1 (c)) instead of HTL (as is commonly used), to maintain not only an adequate charge balance in OLED (by choosing the NPB thickness value to the one usually used in classic OLED) but also to increase the number of layers for which the thickness can be slightly tuned (+/- 5-10 nm), to exactly achieve the cavity length for MOLED optical optimization. In order to verify the electrical

performances of this optically optimized stack, ITO-based OLED were fabricated and characterized. The obtained devices exhibited 4.7 % maximum external quantum efficiency (EQE) close to the 5% theoretical limit of fluorescent OLEDs (see table 1).

The experimental EL spectra for the 4 designed AZO-based devices are depicted in Fig. 3 (a). As can be seen at the same applied current density (10 mA/cm^2), the peak for the MOLED 1.5 is around 3 times higher than the peak for the classic OLED. This significant improvement is in good agreement with the modelling results. The spectral filtering around 470 nm is also clear compared to the conventional OLED. The peak intensity for higher number of pairs (2.5 and 3.5) is also enhanced at 470 nm but to a lower extent. MOLED 2.5 presents a similar spectral behaviour, but a smaller intensity and a slightly red-shifted emission peak. Finally, a second peak is observed in the range [560-610 nm] for all MOLEDs. As above-mentioned, it corresponds to the upper limit of the DBR spectral band (see Fig. 2 (a)). The resulting parasitic emission in this range is not suited for our optical biosensor application. As expected, its amplitude increases with the number of pairs. Consequently, these measurements confirm that MOLED 1.5 case leads to the best results. As can be seen, the EL spectra of the MOLED 1.5 matches perfectly with the expected shape: a strong enhancement of the emission in the low reflectivity wavelengths around 470 nm and reduced emission in the 500-600 nm bandwidth. It is worth mentioning that the FWHM was reduced from around 74 nm for the classic OLED to 26 nm for the MOLED 1.5. In Fig. 3 (b), pictures of the OLED and MOLED 1.5 are shown, in which the change of the EL spectra can be appreciated simply by observing the color difference with a better color purity for the MOLED.

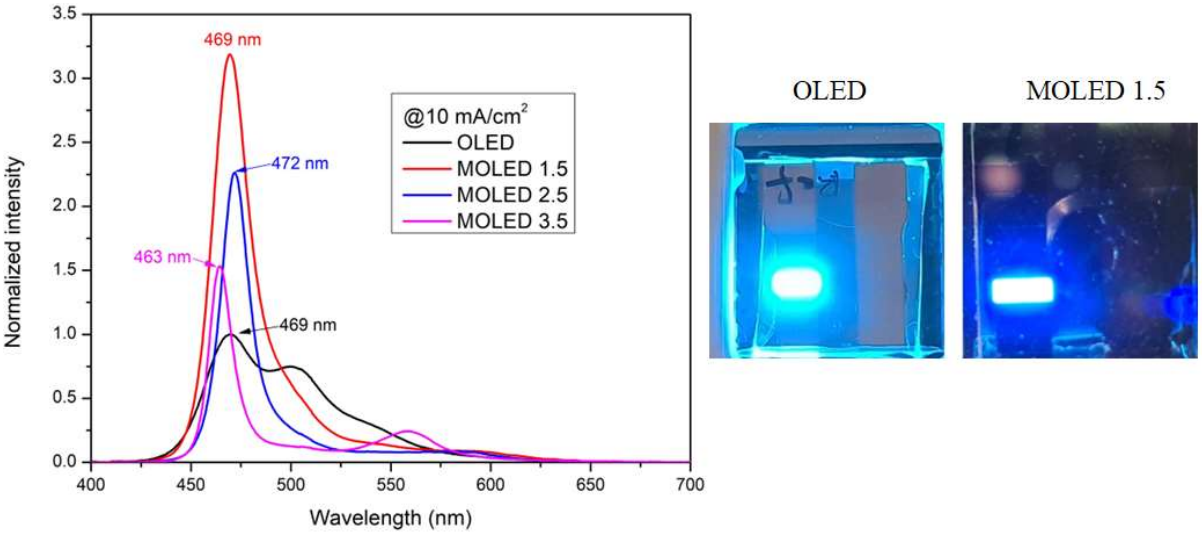

Fig. 3. (a) EL spectra for the classic OLED and the three different MOLEDs (1.5, 2.5 and 3.5) at 10 mA/cm^2. All spectra are normalized with the peak of the classic OLED. (b) Pictures of the OLED and the MOLED 1.5.

Fig. 4 (a) and (b) display the angular dependence of the EL spectra for the standard OLED and MOLED 1.5 respectively. For the OLED the emission peak is slightly shifted and significantly reduced, while the emission intensity after 500 nm reduces but its contribution to the spectrum increases. On the other hand, the MOLED has a significant shift and reduction around its emission peak, while the emission in the 500-600 nm bandwidth remains similar (except at 90° where it is minimal). Fig. 4 (c) and (d) shows the experimental angular dependence of the normalized luminance and EL intensity for OLED and MOLED 1.5 respectively. It can be seen that, the OLED luminance is maximum at 40° and not at 0° as expected for an ideal Lambertian-like pattern emission. This is due to fact that the EL spectra for this blue OLED have a more significant contribution of green wavelengths (520 nm see Fig. 4 (a)) at oblique incidence. The angular distribution of the MOLED 1.5, which emits less in the green region (around 550 nm), has its maximum emission in the 0-20° range and a reduced emission for higher angles due to the microcavity effect. On the other hand, if we measure specifically the angular dependence of the EL intensity for the OLED and MOLED at 470 nm which is the wavelength target for the light excitation source (not taken into account any other wavelength), the effect of the microcavity is clear (**Erreur ! Source du renvoi introuvable.** (d)). This change in the light distribution for the MOLED is highly desirable from the sensor point of view because most of the light will be directed vertically (0°) to the algae.

On the other hand, as the emission is improved about 3 times in the MOLED 1.5 compared with the standard OLED, the current density needed to reach the same peak intensity will be lower. This reduction in the current applied is anticipated to extend the lifetime of the devices by reducing the excited states generated by recombining charges[25].

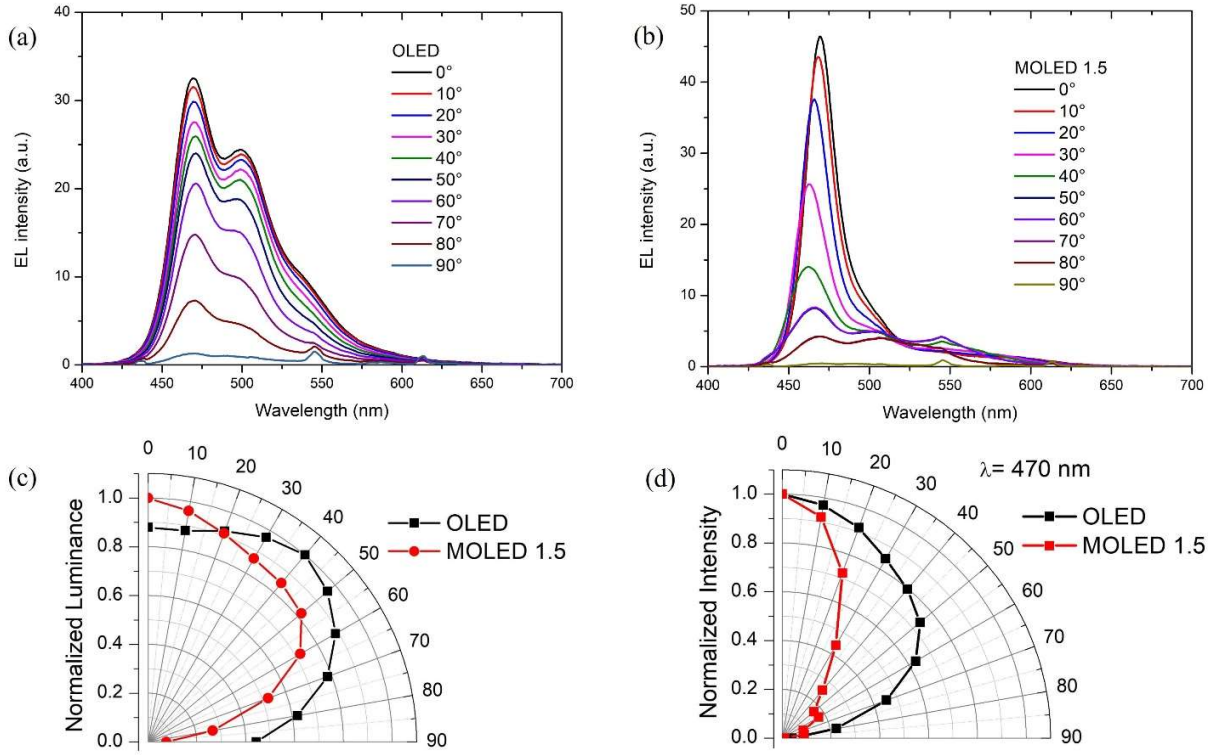

Fig. 4. Angular dependence of (a) the normalized luminance and (b) the normalized EL peak intensity at 470 nm for the OLED and the MOLED 1.5. EL spectra at different angles for (c) the OLED and (d) the MOLED 1.5.

In the Fig. 5 (b), EQE values as a function of the applied current density for the classic OLED and MOLED 1.5 are shown. MOLED 1.5 had a maximum improvement of 33 % compared to the classic OLED. Consequently, despite a reduced FWHM, the MOLED EQE is higher than the OLED one owing to the microcavity effect. Furthermore, the reduction of the necessary current density required to obtain a given luminescence level is expected to extend the lifetime of the devices for the sensor.

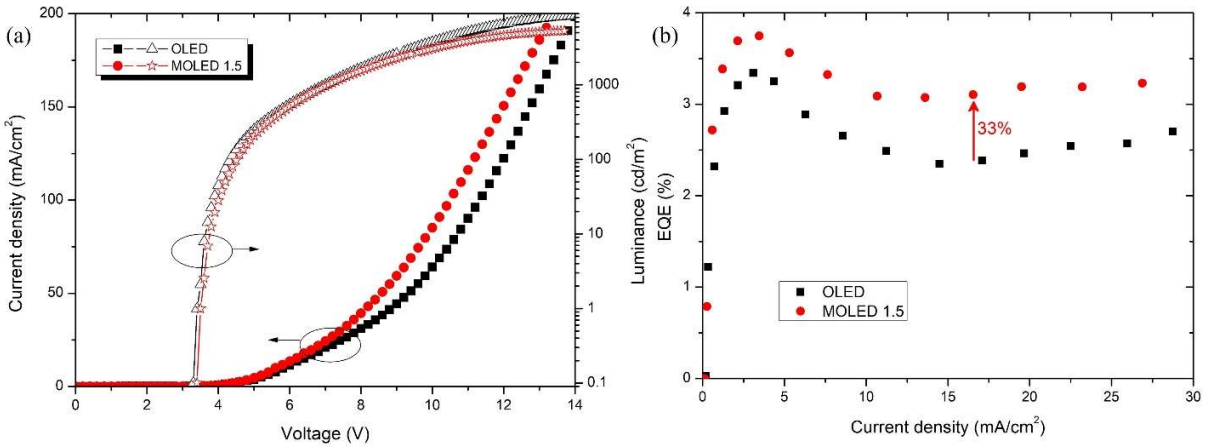

Fig. 5. (a) J-L-V characteristics and (b) the EQE for the classic OLED and the MOLED 1.5.

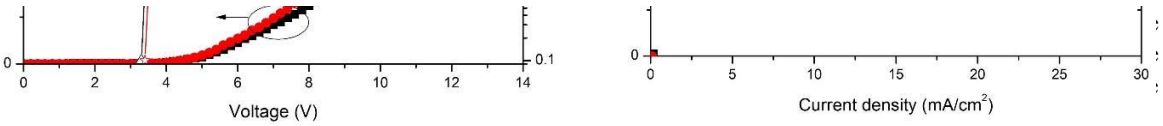

(a)). On the other hand, the EQE_{max} is improved in the MOLED 1.5, from 3.4 to 3.7 %, compared to the value obtained for the OLED even when the luminance of the MOLED 1.5 is lower (5291 cd/m^2 vs 8294 cd/m^2). This is due to the fact the luminance is a measure of light that has a responsivity corresponding to the human eye and is formally known as the CIE photopic luminous efficiency function (V(λ)). Therefore V(λ) has its maximum response around the green wavelengths (555 nm), which are not favoured in the MOLED 1.5 case.

Table 1. Performance of the OLED and MOLED devices.

Device	V_{on} (V)	L_{max} (cd/m^2)	EQE_{max} (%)	EQE_{100}	EQE_{1000}	λ_{peak} (nm)	FWHM (nm)
ITO-OLED	3.1	20166	4.7	4.5	4	469	~74
AZO-OLED	3.3	8294	3.4	3.1	2.4	469	~74
AZO-MOLED 1.5	3.4	5291	3.7	3.7	3.2	469	26

V_{on} = turn-on voltage at 0.1 cd/m^2, L_{max}= maximum luminance, EQE_{max}= maximum external quantum efficiency, EQE_{100}= external quantum efficiency at 100 cd/m^2, EQE_{1000}= external quantum efficiency at 1000 cd/m^2, λ_{peak}= peak of emission

4. Conclusion

In this work, by designing a blue AZO-based MOLED for an optical biosensor, it has been obtained a light excitation source with improved emission in the blue range (470 nm) combined to a low emission in the green region in agreement with the requirements of the aimed algae fluorescence sensor. Exploiting a MOLED, the EQE was improved up to 33 % compared with the reference OLED, while at the same time the FWHM was reduced from about 74 nm to only 26 nm and the angular distribution decreased from 40° to 20°. Further work towards the integration of such light sources into biosensors will focus on the improvement of emission filtering around 600 nm by adding an internal filter in the structure and the study of the device stability and lifetime. In addition, the strategy here followed to find a simultaneous solution for the best OLED stack and the best MOLED design, could be applied in the future for newest and more efficient generation devices (phosphorescent, TADF, hyperfluorescent) once that their stability is comparable with the first generation (fluorescence).

Acknowledgements

We acknowledge financial support by the Agence Nationale de la Recherche (ANR) under the project BELUGA (grant number: ANR-18-CE04-0007). This work was supported by LAAS-CNRS micro and nanotechnology platform, a member of the Renatech French national network. E. Scheid, J. Roul and B. Franc from LAAS-CNRS are also acknowledged for their help on sample characterizations.

References

[1] C.W. Tang, S.A. VanSlyke, Organic electroluminescent diodes, Appl Phys Lett. 51 (1987) 913–915. https://doi.org/10.1063/1.98799.

[2] S.J. Zou, Y. Shen, F.M. Xie, J. de Chen, Y.Q. Li, J.X. Tang, Recent advances in organic light-emitting diodes: toward smart lighting and displays, Mater Chem Front. 4 (2020) 788–820. https://doi.org/10.1039/C9QM00716D.

[3] H. Zhu, Y. Shen, Y. Li, J. Tang, Recent advances in flexible and wearable organic optoelectronic devices, Journal of Semiconductors. 39 (2018) 011011. https://doi.org/10.1088/1674-4926/39/1/011011.

[4] C. Murawski, M.C. Gather, Emerging Biomedical Applications of Organic Light-Emitting Diodes, Adv Opt Mater. 9 (2021) 2100269. https://doi.org/10.1002/ADOM.202100269.

[5] Y. Huang, E.L. Hsiang, M.Y. Deng, S.T. Wu, Mini-LED, Micro-LED and OLED displays: present status and future perspectives, Light: Science & Applications 2020 9:1. 9 (2020) 1–16.

https://doi.org/10.1038/s41377-020-0341-9.
[6] J. Zhao, S. Xie, S. Han, Z. Yang, L. Ye, T. Yang, Organic light-emitting diodes with AZO films as electrodes, Synth Met. 114 (2000) 251–254. https://doi.org/10.1016/S0379-6779(00)00237-X.
[7] G. Hong, X. Gan, C. Leonhardt, Z. Zhang, J. Seibert, J.M. Busch, S. Bräse, G. Hong, X. Gan, C. Leonhardt, Z. Zhang, J. Seibert, J.M. Busch, S. Bräse, A Brief History of OLEDs—Emitter Development and Industry Milestones, Advanced Materials. 33 (2021) 2005630. https://doi.org/10.1002/ADMA.202005630.
[8] A. Monkman, Why Do We Still Need a Stable Long Lifetime Deep Blue OLED Emitter?, ACS Appl Mater Interfaces. 14 (2021). https://doi.org/10.1021/ACSAMI.1C09189/ASSET/IMAGES/LARGE/AM1C09189_0001.JPEG.
[9] C.Y. Chan, M. Tanaka, Y.T. Lee, Y.W. Wong, H. Nakanotani, T. Hatakeyama, C. Adachi, Stable pure-blue hyperfluorescence organic light-emitting diodes with high-efficiency and narrow emission, Nature Photonics 2021 15:3. 15 (2021) 203–207. https://doi.org/10.1038/s41566-020-00745-z.
[10] Q. Zhang, D. Zhang, Y. Fu, S. Poddar, L. Shu, X. Mo, Z. Fan, Light Out-Coupling Management in Perovskite LEDs—What Can We Learn from the Past?, Adv Funct Mater. 30 (2020) 2002570. https://doi.org/10.1002/ADFM.202002570.
[11] R.H. Jordan, L.J. Rothberg, A. Dodabalapur, R.E. Slusher, Efficiency enhancement of microcavity organic light emitting diodes, Appl Phys Lett. 69 (1996) 1997–1999. https://doi.org/10.1063/1.116858.
[12] X. Huang, Y. Qu, D. Fan, J. Kim, S.R. Forrest, Ultrathin, lightweight and flexible organic light-emitting devices with a high light outcoupling efficiency, Org Electron. 69 (2019) 297–300. https://doi.org/10.1016/J.ORGEL.2019.03.040.
[13] Y.J. Pu, G. Nakata, F. Satoh, H. Sasabe, D. Yokoyama, J. Kido, Optimizing the Charge Balance of Fluorescent Organic Light-Emitting Devices to Achieve High External Quantum Efficiency Beyond the Conventional Upper Limit, Advanced Materials. 24 (2012) 1765–1770. https://doi.org/10.1002/ADMA.201104403.
[14] J. Lin, Y. Hu, X. Liu, Microcavity-Enhanced Blue Organic Light-Emitting Diode for High-Quality Monochromatic Light Source with Nonquarterwave Structural Design, Adv Opt Mater. 8 (2020) 1901421. https://doi.org/10.1002/ADOM.201901421.
[15] T.Y. Cho, C.L. Lin, C.C. Wu, Microcavity two-unit tandem organic light-emitting devices having a high efficiency, Appl Phys Lett. 88 (2006) 111106. https://doi.org/10.1063/1.2185077.
[16] M. Chakaroun, A.T. Diallo, S. Hamdad, S. Khadir, A.P.A. Fischer, A. Boudrioua, Experimental and theoretical study of the optical properties optimization of an OLED in a microcavity, IEEE Trans Electron Devices. 65 (2018) 4897–4904. https://doi.org/10.1109/TED.2018.2870070.
[17] B. Dugrenil, I. Séguy, H.-Y. Lee, T. Camps, Y.-C. Lin, J.B. Doucet, Y.-S. Chiu, L. Salvagnac, E. Bedel-Pereira, M. Ternisien, C.T. Lee, V. Bardinal, AZO electrodes deposited by atomic layer deposition for OLED fabrication, Https://Doi.Org/10.1117/12.2052504. 9137 (2014) 127–132. https://doi.org/10.1117/12.2052504.
[18] Q. Feng, W. Wang, K. Jiang, J. Huang, Y. Zhang, W. Song, R. Tan, Effect of deposition condition and UV-ozone post-treatment on work function of DC magnetron sputtered AZO thin films, Journal of Materials Science: Materials in Electronics. 23 (2012) 267–272. https://doi.org/10.1007/S10854-011-0400-3/TABLES/3.
[19] M. Shukla, N. Brahme, R.S. Kher, M. Khokhar, Elementary approach to calculate quantum efficiency of polymer light emitting diodes, Undefined. (2011).
[20] Y. Deng, C. Keum, S. Hillebrandt, C. Murawski, M.C. Gather, Improving the Thermal Stability of Top-Emitting Organic Light-Emitting Diodes by Modification of the Anode Interface, Adv Opt Mater. 9 (2021) 2001642. https://doi.org/10.1002/ADOM.202001642.
[21] K. Yamaguchi, Y. Esaki, T. Matsushima, C. Adachi, A 1,4,5,8,9,11-hexaazatriphenylenehexacarbonitrile (HAT-CN) transport layer with high electron mobility for thick organic light-emitting diodes, AIP Adv. 10 (2020) 055304. https://doi.org/10.1063/5.0007310.
[22] C.H. Park, S.W. Kang, S.G. Jung, D.J. Lee, Y.W. Park, B.K. Ju, Enhanced light extraction efficiency and viewing angle characteristics of microcavity OLEDs by using a diffusion layer, Scientific Reports 2021 11:1. 11 (2021) 1–10. https://doi.org/10.1038/s41598-021-82753-9.
[23] H.G. Park, S.G. Park, Electro-Optical Performance of Organic Thin-Film Using HAT(CN)6 between Anode and Organic Materials, Coatings 2019, Vol. 9, Page 648. 9 (2019) 648. https://doi.org/10.3390/COATINGS9100648.
[24] T.Y. Chu, O.K. Song, Hole mobility of N,N′-bis(naphthalen-1-yl)-N,N′-bis(phenyl) benzidine investigated by using space-charge-limited currents, Appl Phys Lett. 90 (2007) 203512.

https://doi.org/10.1063/1.2741055.
[25] D. Chen, F. Zhao, K. Tong, G. Saldanha, C. Liu, Q. Pei, Mitigation of Electrical Failure of Silver Nanowires under Current Flow and the Application for Long Lifetime Organic Light-Emitting Diodes, Adv Electron Mater. 2 (2016) 1600167. https://doi.org/10.1002/AELM.201600167.